ELSEVIER

Engineering Structures 21 (1999) 149–167

ENGINEERING STRUCTURES

Applications of wavelet transforms in earthquake, wind and ocean engineering

Kurtis Gurley, Ahsan Kareem

Department of Civil Engineering and Geological Sciences, University of Notre Dame, Notre Dame, IN 46556, USA

Received December 1996; revised version accepted June 1997

Abstract

The analysis, identification, characterization and simulation of random processes utilizing both the continuous and discrete wavelet transform is addressed. The wavelet transform is used to decompose random processes into localized orthogonal basis functions, providing a convenient format for the modeling, analysis, and simulation of non-stationary processes. The time and frequency analysis made possible by the wavelet transform provides insight into the character of transient signals through time-frequency maps of the time variant spectral decomposition that traditional approaches miss. In the relatively short life of the wavelet transform, it has found use in a wide variety of applications. This applications-orientated paper will briefly discuss the development of the continuous and discrete wavelet transform for digital signal analysis and present numerous examples where the authors have found wavelet analysis useful in their studies concerning the identification and characterization of transient random processes involving ocean engineering, wind and earthquakes.

1. Introduction

Non-stationary signals are frequently encountered in a variety of engineering fields (e.g. wind, ocean, and earthquake engineering). The inability of conventional Fourier analysis to preserve the time dependence and describe the evolutionary spectral characteristics of non-stationary processes requires tools which allow time and frequency localization beyond customary Fourier analysis. The spectral analysis of nonstationary signals cannot describe the local transient features due to averaging over the duration of the signal. For example, the response of a linear system to unit amplitude stationary white noise and the impulse response function of the system will have identical spectral descriptions, but both will have drastically different time histories. One will be characterized by a filtered white noise, while the other will represent a decaying signal. An FFT based method called the short-term Fourier transform (STFT) provides time and frequency localization to establish a local spectrum for any time instant. The key feature of the STFT is the application of the Fourier transform to a time varying signal when the signal is viewed through a narrow window centered at a time t. The local frequency content is then obtained at time t. The window is moved to a new time and the process is repeated. High resolution cannot be obtained in both time and frequency domains simultaneously. The window must be chosen for locating sharp peaks or low frequency features, because of the inverse relation between window length and the corresponding frequency bandwidth [1].

This drawback can be alleviated if one has the flexibility to allow the resolution in time and frequency to vary in the time-frequency plane to reach a multi-resolution representation of the process. Accordingly, the time-frequency window would narrow automatically to observe high frequency contents of a signal and widen to capture low frequency phenomena. This is possible if the analysis is viewed as a filter bank consisting of bandpass filters with constant relative bandwidths. Fourier methods of signal decomposition use infinite sines and cosines as basis functions, whereas the wavelet transform uses a set of orthogonal basis functions which are local. A short duration, high frequency phenomenon is buried in a Fourier representation with the background averaged spectral content, whereas wavelet transformation allows the retention of local transient signal characteristics beyond the capabilities of the infinite harmonic

0141-0296/99/$—see front matter
PII: S0141-0296(97)00139-9

basis functions by allowing a multi-resolution representation of a process.

1.1. Brief wavelet overview

Digital signal analysis using wavelet transforms begins with the generation of a single parent wavelet. The signal is then decomposed into a series of basis functions of finite length consisting of dilated (stretched) and translated (shifted) versions of this parent wavelet function, i.e. wavelets of different scales and positions in time or space. This process is similar to Fourier analysis, where the parent wavelet is analogous to the sine wave, and the basis functions in Fourier decomposition are sine waves of various amplitude, phase and frequency variations of the parent sine wave.

Fig. 1 gives a qualitative outlay of the representation of a random signal using wavelet decomposition and Fourier decomposition. The top plot is the measured response of a structure to environmental loads. The right column shows several sine-wave basis functions of various frequencies used by Fourier analysis. Each wave is represented by a single complex coefficient describing amplitude and phase. The left column is a qualitative view of several wavelet-basis functions that might be used to decompose the structural response. Each of the three plots in the left column consist of multiple translations of a single parent wavelet function, which in this case resembles a windowed sine wave. The first of the three left plots is built from nine parent wavelets, the middle left plot consists of five wavelets, encompassing lower frequency information. The bottom left plot is built from three parent wavelets dilated still larger, capturing even lower frequency behavior. The essential dif-

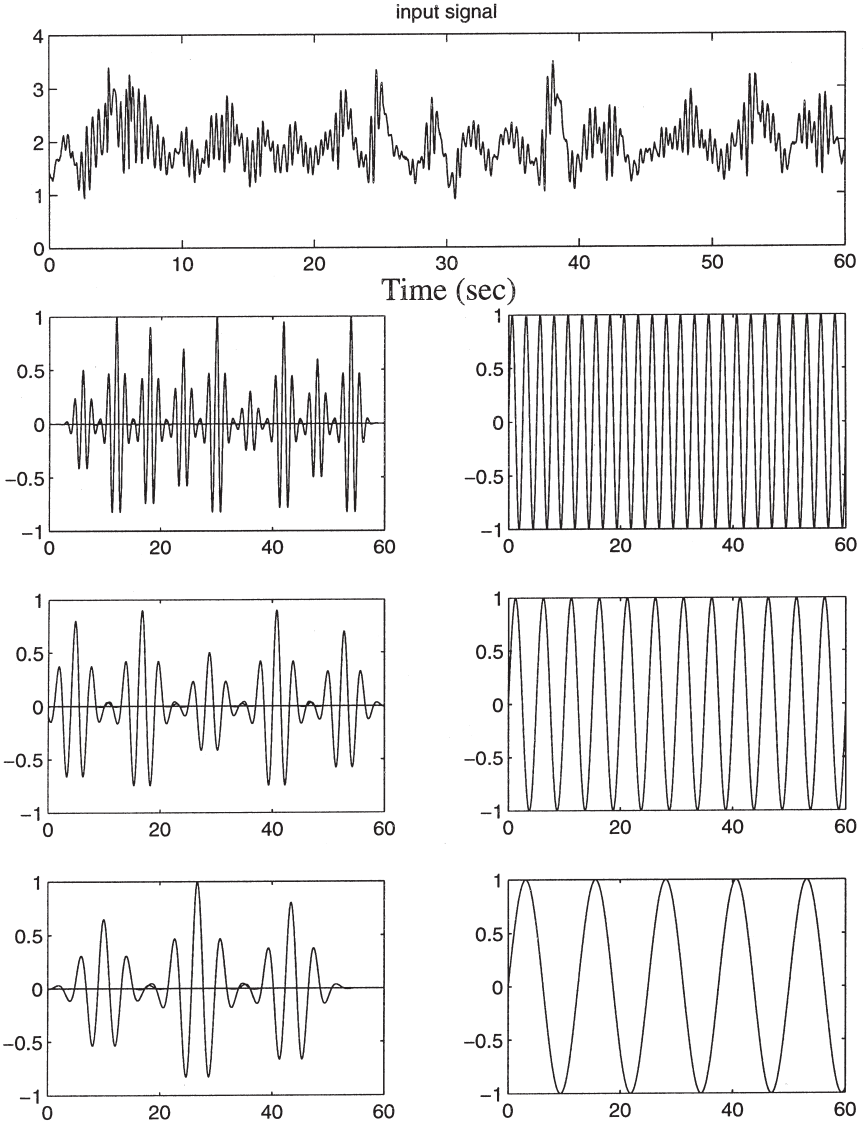

Fig. 1. A structural response signal, a view of the wavelet decomposition basis functions (left column), and a view of the Fourier decomposition basis functions (right column).

ference between wavelet and Fourier analysis is that the wavelet basis function for any frequency band consists of a number of local functions strung together, each with its own amplitude, and can thus distinguish local events at different times at the same frequency. The Fourier basis functions utilize a single function with a single amplitude over the complete time frame at any given frequency. Thus, any transient events are blended into one coefficient, not singled out through multiple coefficients.

There are a variety of parent wavelets available in the literature, each of which has been developed to meet certain criteria. One important property, for example, is that the original signal may be retrieved from the wavelet transform. This invertibility property is achieved by the admissibility condition, which requires the total area under the parent wavelet to be equal to zero. Wavelets must also have finite duration, i.e. finite spatial support. This prevents any localized transient signal features from being propagated in or smeared through time by its wavelet representation [2].

One of the first widely applied parent wavelets was developed by Daubechies [3,4]. Development of this parent wavelet begins with the solution of a dilation equation to determine a scaling function $\phi(n)$, dependent on certain restrictions. The scaling function is used to define the parent wavelet function, $\psi(n)$. The shape of the parent wavelet is not a single unique shape, but depends on the desired wavelet features. For a wavelet of order N, the dilation and wavelet functions are found by the solution to

$$\phi(n) = \sum_{j=0}^{N-1} c_j \phi(2n - j) \text{ and}$$
$$\psi(n) = \sum_{j=0}^{N-1} (-1)^j c_j (2n + j - N + 1) \quad (1)$$

The constraints on the coefficients c_j produce N equations for their solution. The higher the order, the more the parent wavelet approaches a windowed Gaussian weighted harmonic function. The resulting coefficients have been calculated and reported in References 3 and 4.

1.2. The discrete wavelet transform

The wavelet transformation is a process of determining how well a series of wavelet functions represent the signal being analyzed. The goodness of fit of the function to the signal is described by the wavelet coefficients. The result is a bank of coefficients associated with two independent variables, dilation and translation. Translation typically represents time, while scale is a way of viewing frequency content. Larger scales correspond to lower frequencies.

The most efficient and compact form of wavelet analysis is accomplished by decomposing a signal into a subset of translated and dilated parent wavelets, where these various scales and shifts in the parent wavelet are related based on powers of two. Full representation of the signal (and thus possible invertibility) can be achieved using a vector of wavelet coefficients the same length as the signal. Fewer coefficients may be used for compression purposes.

Consider a signal consisting of 2^M data points, where M is an integer. Discrete wavelet transformation (DWT) requires 2^M wavelet coefficients to fully describe the signal. DWT decomposes the signal into $M+1$ levels, where the level is denoted as i, and the levels are numbered $i = -1, 0, 1, \ldots, M-1$. Each level i consists of $j = 2^i$ translated and partially overlapping wavelets equally spaced $2^M/j$ intervals apart. The $j = 2^i$ wavelets at level i are dilated such that an individual wavelet spans $N-1$ of that levels intervals, where N is the order of the wavelet being applied. Each of the $j = 2^i$ wavelets at level i is scaled by a coefficient $a_{i,j}$ determined by the forward wavelet transform, a convolution of the signal with the wavelet. The notation is such that i corresponds to the wavelet dilation, and j is the wavelet translation in level i. $a_{i,j}$ is often written as a vector a_{2^i+j}, where $j = 0, 1, \ldots, i-1$. The level $i = -1$ is the signal mean value [5].

The forward wavelet transform determines the wavelet coefficients, $a_{i,j}$ of the j wavelets at each level i. For the signal $f(n)$, the DWT is

$$a_{i,j} = a_{2^i+j} = \sum_n f(n)\psi_{i,j}(n) \quad (2)$$

and the corresponding inverse wavelet transform IWT is

$$f(n) = \sum_i \sum_j a_{i,j}\psi_{i,j}(n), \quad (3)$$
$$\text{where } \psi_{i,j}(n) = 2^{i/2}\psi(2^i n - j)$$

A DWT algorithm was developed by Mallet [6], which computes the solution of equation (2) without solving for either $\phi(n)$, or $\psi(n)$ directly. The algorithm uses a series of high and low pass filters to progressively find the wavelet coefficients, $a_{i,j}$, from the highest i level to the mean value level. In the first iteration, the upper half of the frequency content is filtered from the original signal. The high pass signal is used to generate the 2^{M-1} wavelet coefficients that describe the high detail portion of the signal. The low pass filtered data is sent to the next iteration. In the next iteration the upper one half of the remaining frequency content of the signal is high pass filtered once again, this time to generate the next 2^{M-2} wavelet coefficients. The iterations continue until all 2^M wavelet coefficients are determined. This is

referred to as Mallet's tree algorithm or Mallet's pyramid algorithm [6].

1.3. The continuous wavelet transform

While the DWT is the most efficient and compact, its power of two relationship in scale fixes its frequency resolution. Often it is desired to differentiate between smaller frequency bands than DWT allows. This is possible by using scales that are more closely spaced together than the 2^i relationship, and is the basis for the continuous wavelet transform (CWT). The form of the CWT is

$$a(i,j) = \int_{-\infty}^{\infty} f(t)\psi(i,j,t)\,\mathrm{d}t \tag{4}$$

where i corresponds to dilation, and j to translation. For a finite digitally sampled signal, the integral will be replaced with a summation, and the time t is replaced by the discrete n.

The scale may be selected over whatever range the user desires. The number of coefficients necessary to describe the signal may be very much larger than the signal length, as the CWT oversamples the signal and wavelet coefficients contain partial redundancies of information. Also, CWT need not contain information over the complete range of frequencies contained in the signal. The user may select a very narrow range of scales to isolate and pull details from a particular frequency band. In this case the complete signal can no longer be retrieved, since any information in unsampled scales is lost.

2. Applications of wavelet analysis

The present research concerns the use of wavelets to aid in the analysis and simulation of non-stationary data. Multi-scale decomposition of processes utilizing wavelets reveals events otherwise hidden in the original time history. The wavelet coefficients, $a_{i,j}$, can be utilized in a variety of techniques to draw out useful signal information. Wavelet coefficients may be used to derive an estimate of the power spectrum. The wavelet coefficients also provide the scalogram, which describes the signal energy on a time-scale domain. This facilitates identification of time-varying energy flux, spectral evolution, and transient bursts not readily discernible using time or frequency domain methods. The property of accurate energy representation lends itself well to signal reconstruction and simulation. The reduction of noise in a measured signal may be accomplished by altering wavelet coefficients below a case specific threshold. A variety of examples are provided herein to demonstrate these engineering applications of wavelet transforms.

2.1. Wavelet filterbank signal decomposition

The DWT is a convenient and efficient method of monitoring the performance of time dependent dynamic systems. While Fourier coefficients do not contain time information, the coefficients describing the localized basis functions do reflect time dependence. Both the bank of octave band filtered time series, and their wavelet domain representation as wavelet coefficients provide unique insights into transient events within a time series. An example of each is provided below.

2.1.1. Bandpass filtering/offshore platform response to wind and waves

Fig. 2 presents the time history of the response of a large floating offshore structure known as a tension leg platform (TLP) to wind and wave loads in the horizontal plane, and the band-passed time histories using a DWT based filterbank. This figure unfolds the response time history into a very revealing display of the time-scale representation. The top left block is the mean removed original signal, the plots following column-wise downward are the band-pass filtered signal in order of decreasing frequency. Note the different scales on the plots for the filtered processes, indicating relative contribution in that frequency band. The power spectral density of the signal in Fig. 2 is shown in Fig. 3, on which the frequency bands 1 through 7 of the filtered process are marked. The higher relative magnitude of bands 3 and 4 correspond to the right peak in the spectrum, and is due to first-order wave effects. The high relative magnitude in bands 6 and 7 correspond to structural resonance due to wind and second-order wave effects. The wavelet based filter bank has helped to identify, e.g. high frequency spikes and their time of occurrence, associated with waves slamming the deck structure, observed in bands 1 and 2. The origins of these extreme response events in the response of the TLP are not clearly discernible from the complete time history. Large excursions may be due to either high frequency impact loading-type wave slamming events, or to lower frequency hydrodynamic loads on the below-deck structure associated with the passage of large, but not slamming waves. The improved efficiency over FFT and other filtering techniques, e.g. multifiltering with simple oscillators [e.g. Reference 7], renders wavelet filterbanks a quick and convenient time-scale decomposition method.

Wavelet coefficients in specific octaves may be used to monitor system performance as well. The occurrence of large magnitude coefficients in the wavelet domain may be used to identify the isolated impulsive events such as the slamming of waves observed in the previous example. In Fig. 4, the measured pitch rotational response of the TLP is presented along with two selected bands of wavelet coefficients from a discrete wavelet analysis of the response. The top plot is the time record

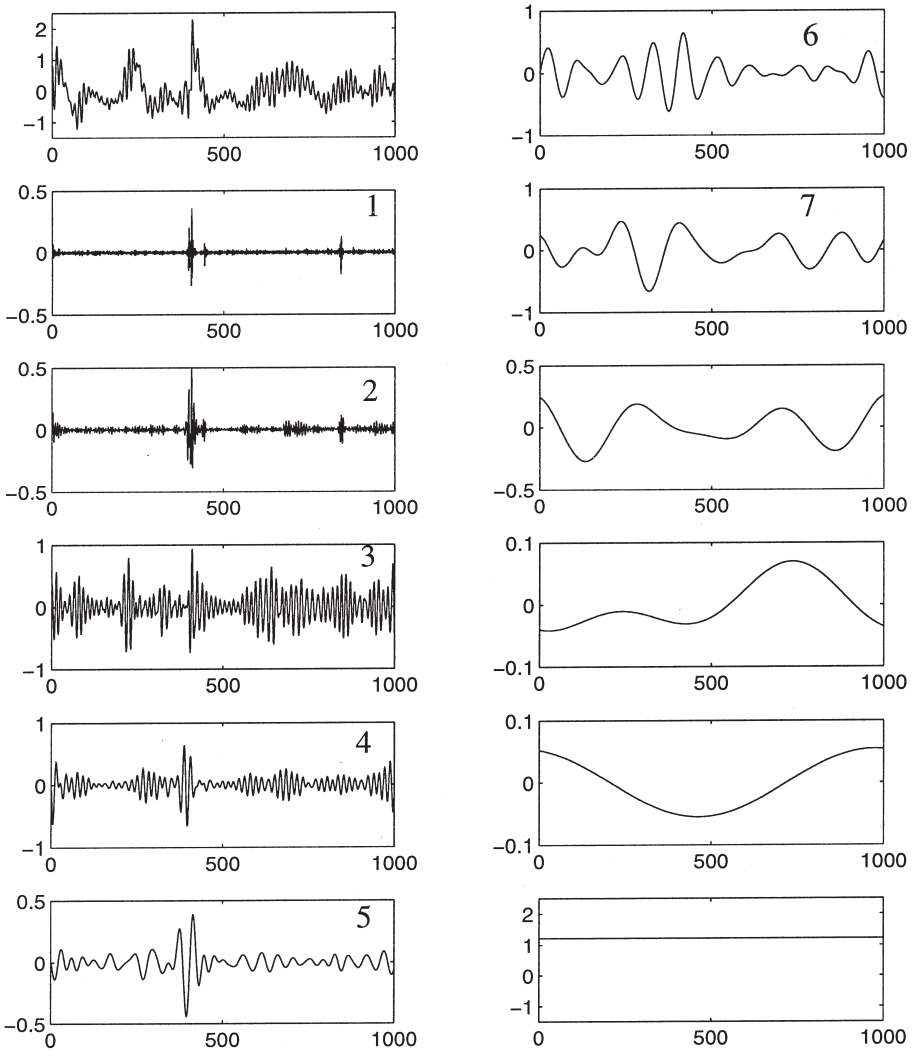

Fig. 2. From top left column-wise downward: measured TLP sure response to wind and wave field and its time-scale decomposition using wavelet transforms.

of pitch response. The second and third plots are the wavelet coefficients corresponding to the highest octave band and the octave band which includes the dominant frequency of incoming waves, respectively. Many spikes are observable in the time record, indicating large pitch response excursions. The spikes in the bottom plot are large magnitude events within the wave frequency band and include large waves on both the below deck and topside structure. The wavelet coefficient spikes in the highest octave are due to sudden high frequency impulse events and indicate wave slamming on the deck structure. Thus, the wavelet coefficients help to distinguish those extreme excursions due to the passage of large waves and their associated loads on the below-deck TLP structure from those due to the sudden impact of large waves on the topside structure.

2.2. Power spectral density estimation

The wavelet coefficients are used to estimate the power spectrum by summing the squared coefficients in each octave, as shown schematically in Fig. 5. In the case of the compact DWT, the wavelet estimation of the spectrum of a signal of length 2^M over the entire frequency range consists of a vector of length M, whose contents are the sum of the square of the wavelet coefficients corresponding to the M octaves. The sampling rate of the frequency band is included as Δt, and the spectral estimate for the ith level is

$$S_i = 2^{i+2-M}\,\Delta t \sum_{j=1}^{2^i} (a_{i,j})^2,\ i = 0, 1, \ldots, M-1 \qquad (5)$$

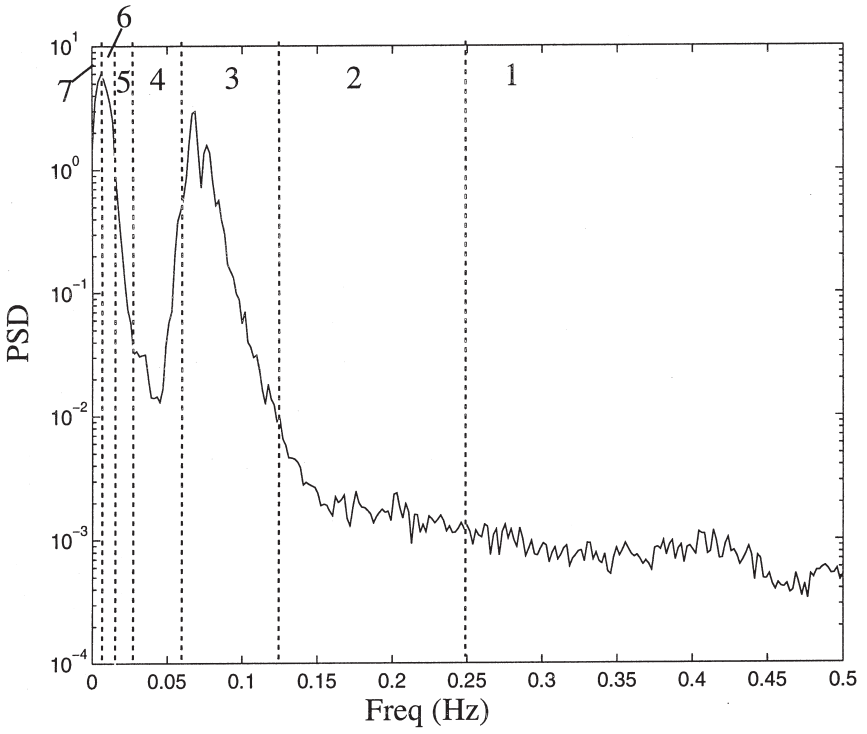

Fig. 3. Power spectral density of measured TLP surge response seen in Fig. 2.

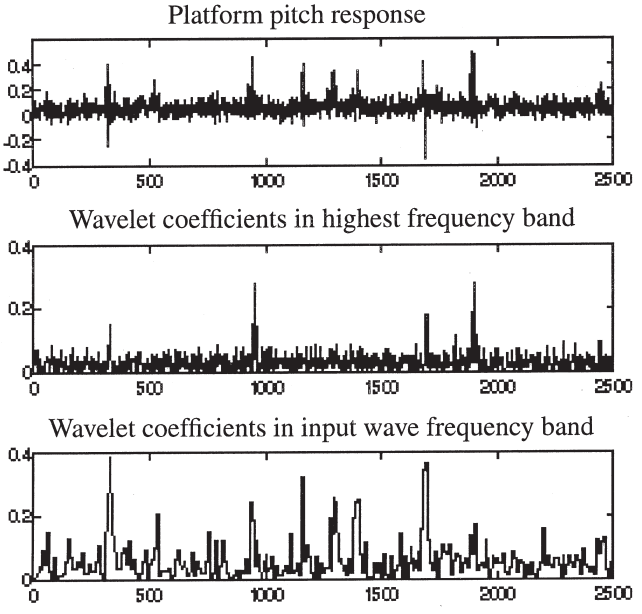

Fig. 4. TLP pitch response, high frequency wavelet coefficient, and wave frequency wavelet coefficients.

The frequency band D_i corresponding to S_i is

$$D_i = \left[\frac{0.5}{\Delta t 2^{i+1}}, \frac{0.5}{\Delta t 2^{i}} \right] \tag{6}$$

A cospectral estimate between two processes is also possible by replacing the squared coefficient term with the product of both process coefficients.

The energy in the DWT spectral estimation closely predicts the actual signal energy, but lacks the resolution available to the FFT methods, particularly in the high frequency range. While it is possible to apply CWT with higher resolution, this problem may also be overcome with the DWT by the use of a prototype wavelet which is slightly dilated with respect to the original parent wavelet. This is done by replacing the wavelet $2^i\psi(2^i n - j)$ by $2^{i+p/P}\psi[2^{i+p/P}(n - j2^i)]$, where P is the desired number of intra-octave estimates,and $p = 0, 1, \ldots, P-1$. The DWT is then run P times, incrementing p from 0 to $P-1$. Using this grid, which is more dense than the octave by octave grid, is equivalent to an over-sampling of the $a_{i,j}$ coefficients [8].

Another option is the application of standard zoom techniques to the octave band passed data. The sequentially high pass filtered processes are shifted to lower frequencies, where further DWT on this zoomed data resolves more detail in the lower octaves. This method is similar to another technique known as wavelet packet analysis [9,10]. The DWT proceeds by a series of low and high pass filters, each in sequence operating on the low pass filtered results of the previous filter, with the high pass results being used to generate the wavelet coefficients. Wavelet packet analysis, while progressively filtering the previous low pass filter results, also filters the high pass filter remainder using DWT, rather

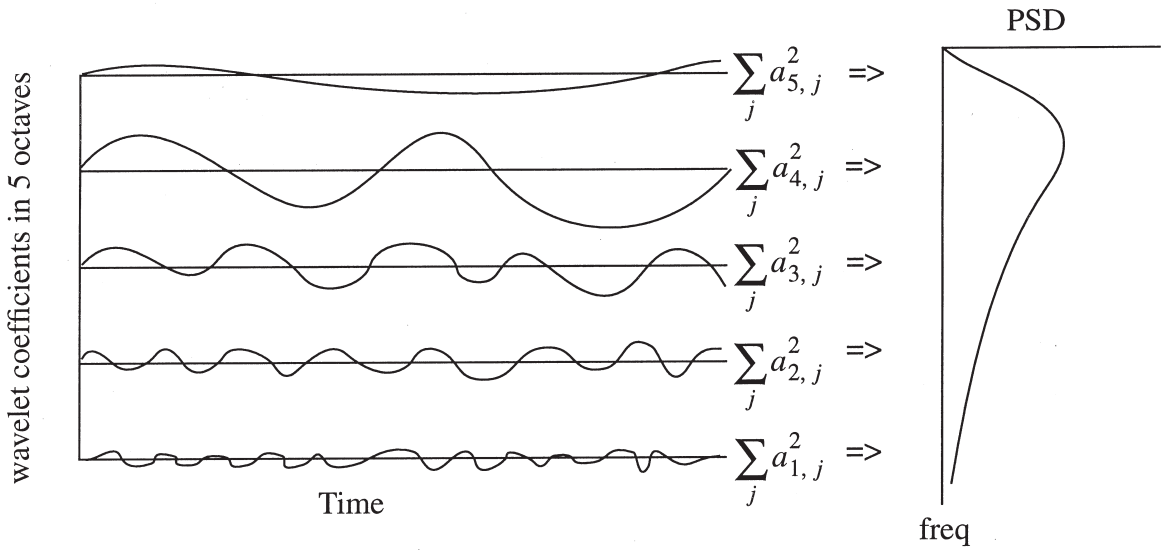

Fig. 5. Summation of wavelet coefficients to estimate power spectrum.

than using the high pass results to generate coefficients. The octave-banded signal information offered by DWT is thus further split up into sub-octaves using wavelet packets.

Fig. 6 shows several power spectrum estimates of a measured earthquake acceleration record. Included are an FFT estimate, an octave band estimate using DWT, and an intra-octave band estimate using DWT and zooming techniques. Fig. 7 is the cospectral estimate of TLP surge response and the measured input wind velocity input using DWT and FFT techniques. Smoothing of the FFT estimate with segment averaging renders its resolution inferior to that of the wavelet estimate at low frequencies. The FFT spectral estimates are the average of eight segments, while the wavelet estimate is based on the full data record.

2.3. Time-frequency signal representation: scalogram

The local wavelet coefficients are well suited for analyzing non-stationary events such as transient and evolutionary phenomena. For DWT there are 2^i coefficients to describe the energy at the ith frequency band, for $i = 0, 1, \ldots, M-1$, where the signal consists of 2^M data

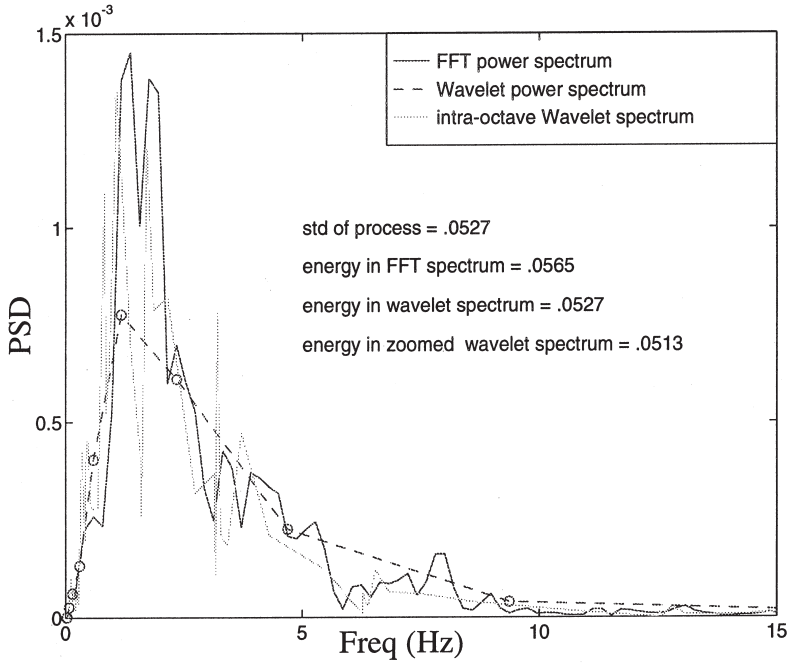

Fig. 6. Wavelet and FFT based spectral estimations of earthquake acceleration record.

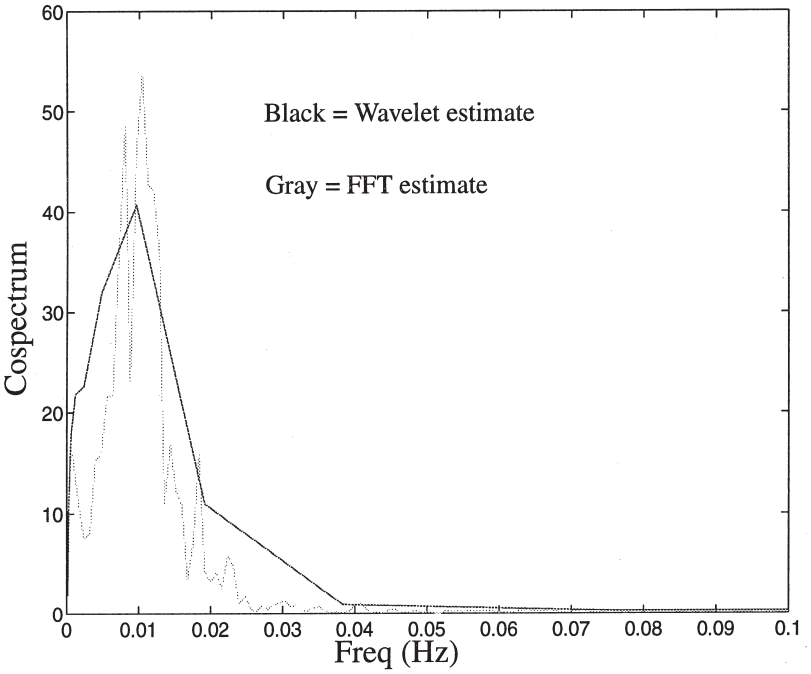

Fig. 7. Cospectrum of wind input and TLP surge response using FFT and wavelet transform estimation.

points. The coefficients in a particular band represent the energy at time intervals equally spaced over the duration of the signal. When the squared coefficients are plotted on a time-scale grid, the transfer of energy from one band to the next may be observed along the time scale. This is called the scalogram or mean square map. The volume bounded by the surface is the mean square value of the signal. The scalogram is easily extended to CWT, where less compact representation is traded for better resolution.

Examples of scalograms are shown in Figs. 8 and 9. In Fig. 8 the analyzed signal in the top plot is a sine wave of constant amplitude and modulated frequency. The second plot in Fig. 8 is a DWT scalogram of the signal, where the horizontal axis is time, and the vertical axis is scale. Note that frequency is inversely proportional to the scale value, thus high frequency is seen at the bottom of the scalogram at low scale values. The transfer of energy from lower to higher frequencies in time is clearly demonstrated as the dark region. The third plot is a CWT scalogram, where more levels between the octaves are added to better delineate the transfer of energy in the signal from low to high frequency. In the fourth plot, a CWT is applied to the signal with an additional high frequency noise added from 1000 to 1200. The added noise magnitude is too small to be detected in the time history, but clearly shows up in the scalogram in the lowest level.

In Fig. 9, the analyzed signal is a hurricane velocity record. Pockets of higher and lower levels of energy in time can be observed in various scales, characterizing the transient nature of convective turbulence in hurricane wind.

The unavoidable presence of noise in measured signals tends to reduce the clarity of scalograms, and in some cases may hide fine structure in coefficient amplitude variation. Denoising, or cleaning noisy signals, is one possible approach to improving the clarity of wavelet analysis, and some DWT based denoising techniques are addressed in a later section. A simple approach to removing noise distortion in scalograms is to remove all coefficients below a certain percentage of the maximum coefficient amplitude when plotting the scalogram. An example can be seen in Reference 11, where a seismic event is analyzed via CWT. Insight into possible physical interpretations of the scalogram are made possible by plotting only those wavelet coefficients within 5 dB of the maximum amplitude.

2.4. Scalogram applications

2.4.1. Structural performance/nondestructive testing

The scalogram reveals much information about the nature of non-stationary processes that was previously hidden. An example application is the diagnosis of special events in structural behavior during earthquake excitation. Any change in frequency content, e.g. initiation of stiffness degradation, sudden occurrence of non-ductile events, energy exchange between modes through response coupling, or pounding between structural components can be identified by the scalogram. Referring to Fig. 10, the wavelet scalogram of ground acceler-

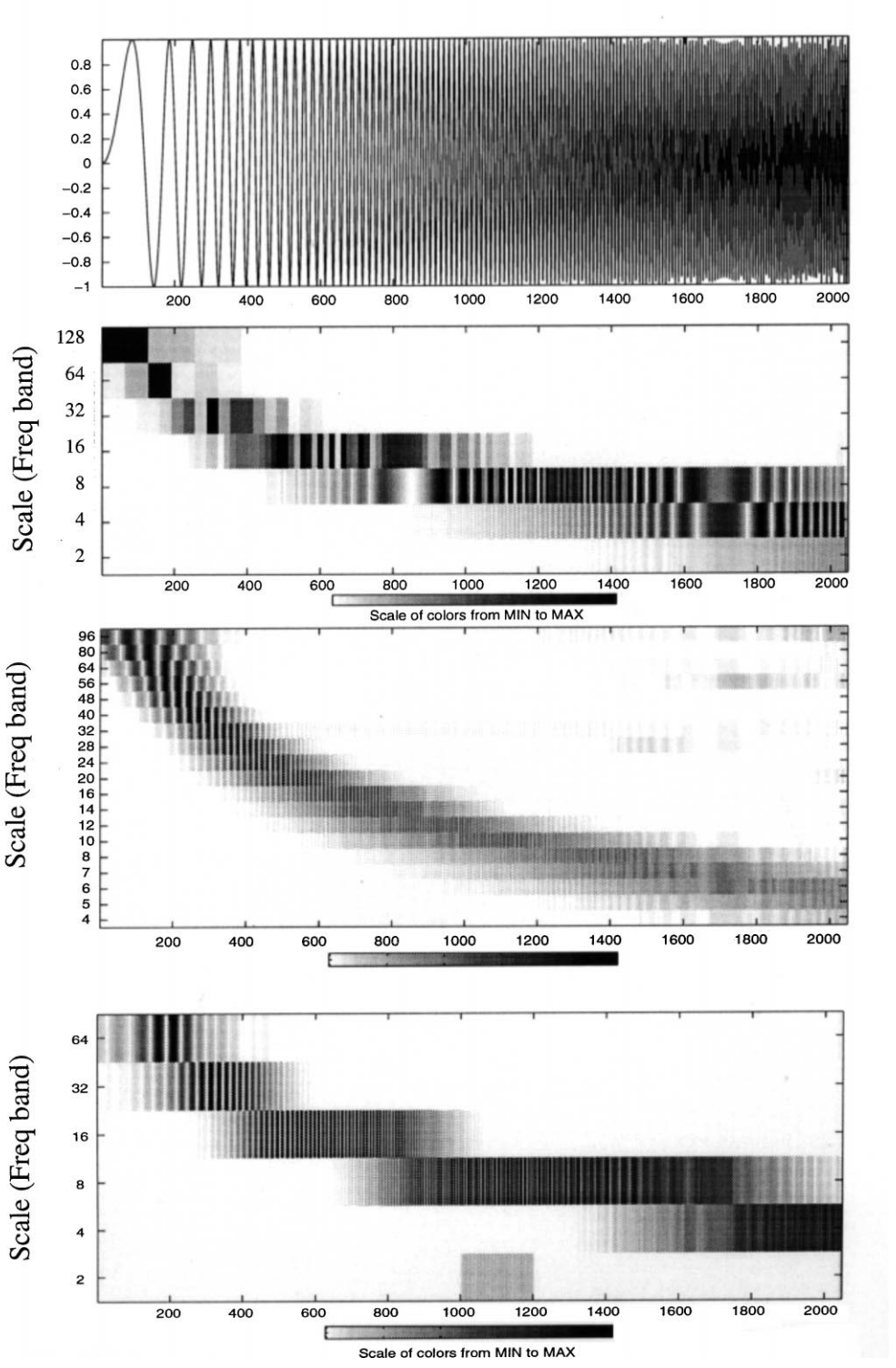

Fig. 8. Frequency modulated sine wave, DWT-scalogram, CWT-scalogram, and CWT-scalogram with high frequency transient noise added to signal between 1000 and 1200.

ation indicates the presence of high frequency energy early in the record which attenuates with time. The presence of high frequency energy will tend to excite higher structural modes. This information may be useful in predicting the building response modes that may be excited during similar earthquakes and the time such excitation begins. The monitoring of such performance information is not available via STFT due to the inflexibility of the time-frequency window which precludes identification of discontinuities in a signal. A multifilter approach util-

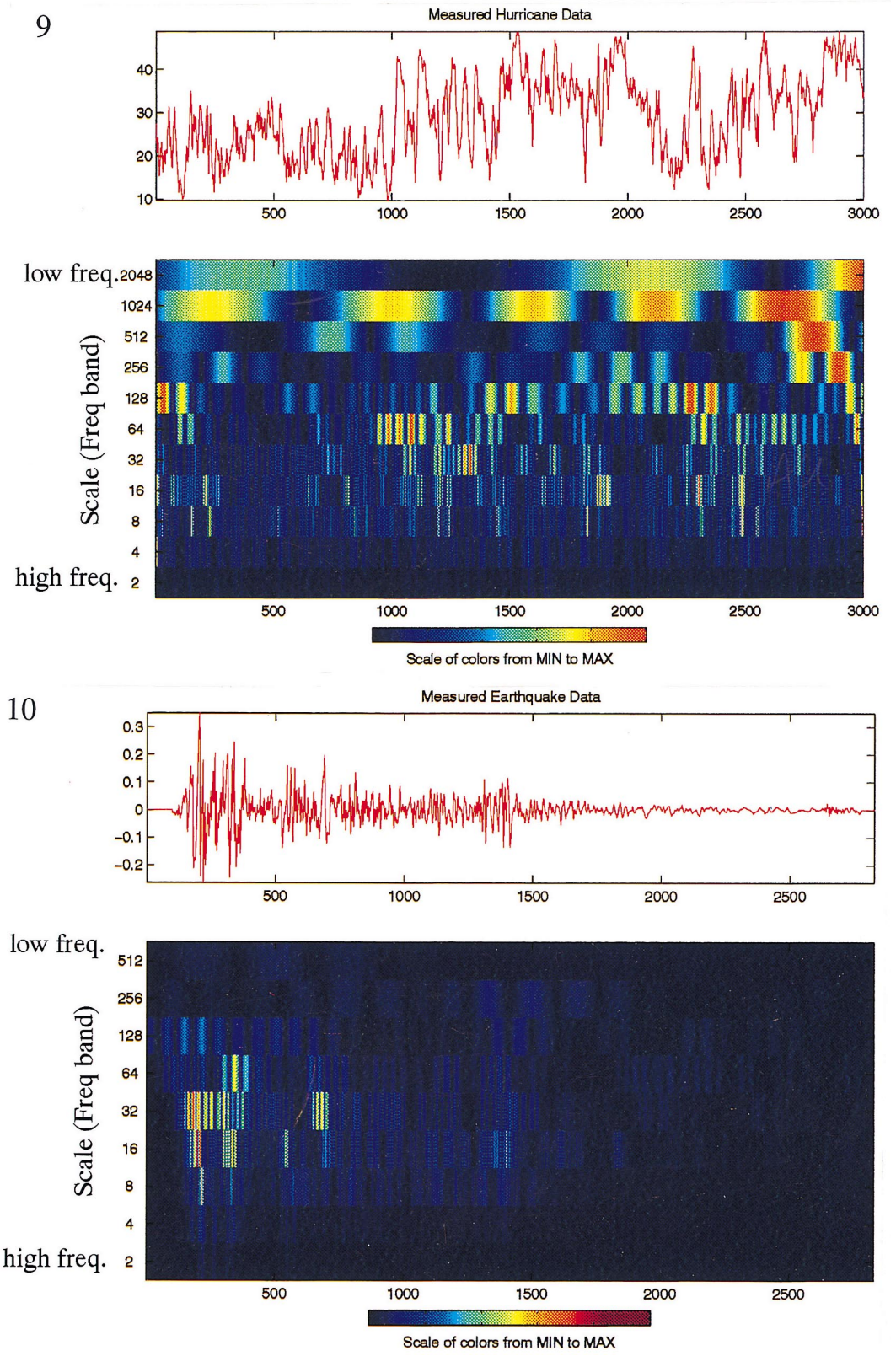

Fig. 9. Measured hurricane data and CWT-scalogram.
Fig. 10. Ground motion record and wavelet scalogram.

izing simple oscillators has been addressed by other researchers to avoid the STFT shortcomings and present time dependent frequency fluctuations [7,12]. This approach has its own shortcomings which are discussed later in the paper.

The propagation of waves in a medium of a structure is widely studied in engineering and science, namely, identification of material properties, crack detection and health monitoring of structures via ultrasound, and monitoring the structural vibration characteristics using impact type techniques. Central to most techniques is the quantification of dispersive features of wave propagation in structures, i.e. wave velocity at different frequencies. The time-frequency analysis offers a most attractive tool for examining and mapping wave propagation at different frequencies. Hodges et al. [13] utilized a STFT approach for the analysis of a string, at beam and a cylindrical shell. By measuring strain at two locations on a structure excited by an arbitrary impact force, travel times of waves between the measurement locations were obtained from the peaks in the time-frequency plots. In their study, a shortcoming was noted in this approach due to inflexibility in the arbitrary selection of time and frequency resolutions. This can be attributed to the fact that the time window for the STFT can either be chosen for resolving sharp local peaks or for identifying low frequency features, but it is impossible to accommodate both desired features due to Heisenberg's uncertainty principle [14,15]. An improvement is possible using Wigner–Ville Distribution, but this approach has its limitations as well [16]. The wavelet transform offers alternative techniques by providing additional flexibility in terms of allowing the resolution in time and frequency to vary in the time-frequency plane, thus considerably reducing analysis.

2.4.2. Ground motion analysis

The time-dependent frequency content of ground motion records provides information on the non-stationary spectral characteristics of the motion, i.e. frequency dependence of ground motion durations, time above a threshold, interval duration, shape wave duration, and identification of energy bursts in the signature. The time-frequency analysis of non-stationary ground motion records has been undertaken by researchers using a multifilter approach [7,12]. The STFT technique has its shortcomings due to the fixed time-frequency relations as alluded to earlier. Following Arnold [17], multifilter techniques have been employed in seismic applications. A set of simple oscillators is used as a multifilter [7]. This approach has the advantage over STFT techniques as a constant damping in the oscillators has the same effect as varying the length of the data window such that it is inversely proportional to frequency. As noted earlier, this is a desired feature for obtaining details of time variations in the high frequency range. Kameda [7] also formulates an evolutionary power spectrum in terms of filter outputs. Scherer [12] utilizes this approach to obtain time-frequency contours of the evolutionary power spectra. Here, the shortcoming of time leakage is reduced by approximating and removing the effects of filter inertness. The application of wavelet analysis will improve resolution while reducing the leakage, thus rendering a wavelet based method as the tool of choice for a time-frequency analysis of ground motion. Fig. 10 illustrates a time-frequency description of the 1940 El Centro earthquake. The El Centro ground motion record contains energy at a wide band of frequencies which may result in exciting higher modes of a building depending on the energy distribution. The arrival of energy bursts at different times can be noted in the time history and more clearly from the scalogram. Wavelet based analysis may lead to improved understanding of the events noted in ground motion in light of geophysical reasoning that relates these energy bursts to S-wave arrivals. Similar results are presented by Sherer et al. [18] using a multifilter technique. However, the present approach offers more flexibility and versatility to analyze a wide range of records with varying frequency contents.

2.4.3. Transient building response to wind storms

Wavelet analysis of hurricane wind time histories, which contain significant contributions from convective turbulence, provides useful information regarding the distribution of energy as a function of time. The response of a slender structure to wind may contain contributions from the fundamental mode and higher modes depending on how the turbulent structure of the wind changes in time. The relative contribution of each mode may vary significantly or the total building response may suddenly increase for apparently the same mean wind speed due to instantaneous changes in the distribution of energy at different frequencies. Such a response behavior cannot be identified through classical spectral techniques, while wavelet analysis is ideal for such an analysis.

As an example, a 600 ft tall, 100 ft square, building is modeled with five modes, and subjected to high (100 ft/sec at 30 ft) wind as correlated point loads along its face. Fig. 11 is a scalogram of the response at the top floor of the building for two input cases. The scalogram plots energy with respect to time (x-axis) and scale (y-axis), where here the scale is marked as levels. The levels 1 through five are five frequency bands, with level 1 containing energy from one half the cutoff frequency up to the cutoff. Level 2 contains energy from 1/4 to 1/2 of cutoff, and so on. Levels 2 through 5 contain all five modes of building response, with the fundamental mode in the 5th level, the second mode in the 4th level, the third and fourth modes in level 3, and the highest mode in level 2. The top plot in Fig. 11 is the response of the top floor to stationary input. The middle

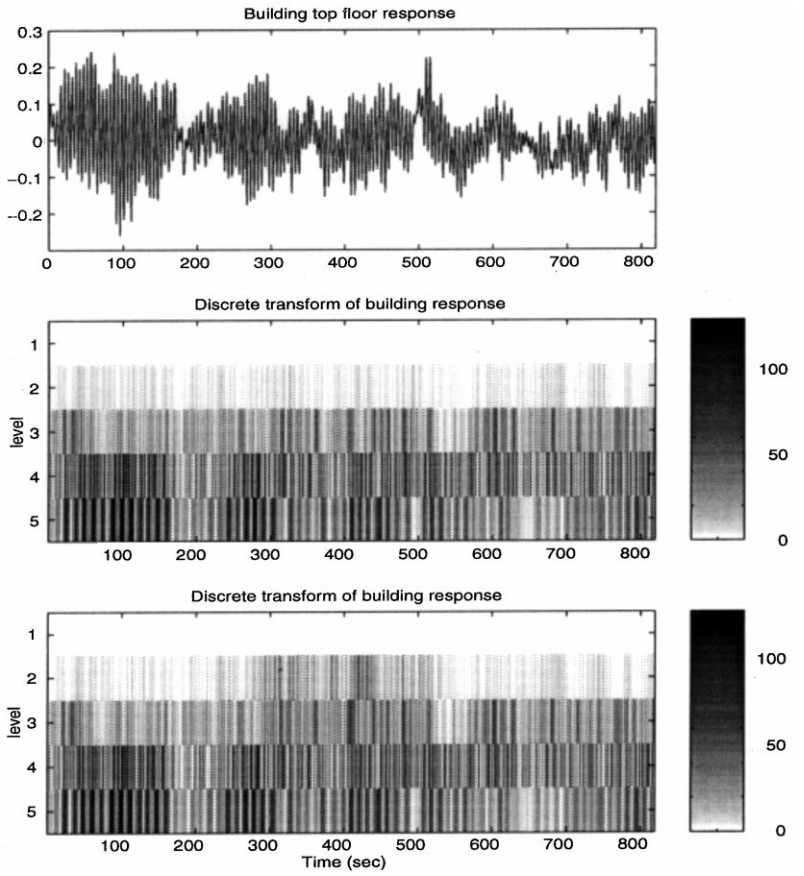

Fig. 11. Top floor building response to hurricane wind (top), scalogram of top floor response to stationary wind (middle), and scalogram of top floor response to wind with transient high frequency fluctuations (bottom).

picture is the scalogram of the 5th floor response to stationary data. The fundamental mode is represented by the darkest band seen in the 5th level, while the 5th mode at level 2 is hardly visible. The bottom picture is the top floor response scalogram when the wind input contains a transient burst of high frequency fluctuations which stimulates the 5th mode for a short duration, visible as level 2 darkens then lightens with time between 300 and 500 s. The response with transient energy in the fifth mode is indistinguishable from the response to stationary wind using Fourier methods or viewing the time histories, while the wavelet transformation clearly brings out the transient characteristics.

2.4.4. Identification of correlation through coscalogram: a wind/pressure example

The scalogram provides the energy evolution with time in a single process by viewing a map of the square of the wavelet coefficients. If the squared coefficient value is replaced with the product of the wavelet coefficients of two different processes, the result is a view of the correlation between the processes. This is called the coscalogram, analogous to the cospectrum in spectral analysis. Like the scalogram, it has the advantage of revealing time varying pockets of high and low correlation in different frequency bands.

Measured full scale wind data is used to demonstrate the application of the coscalogram. Pressure measured on the rooftop of a full scale building and wind velocity measured upstream of the building are utilized in two examples. The first example is seen in the three plots on the left column of Fig. 12, where the scalogram of wind velocity and simultaneously measured pressure are presented along with their coscalogram. It is known that these two records are only slightly correlated, and light patches in the coscalogram help to identify areas of correlation. The right side of Fig. 12 is the scalogram of a different wind velocity record and the same pressure record as the left side example. In this case the wind velocity was measured at a different time, and is not related to the pressure record. The resulting coscalogram of these two unrelated processes in the bottom right corner shows no distinct correlation. Initial analysis shows little correlation between the incident turbulence and the pressure in separated flow regions, suggesting the presence of more complex interactions. Nonetheless, wavelet transforms provide a tool for delineating any relationship between intermittence at certain wave lengths in the

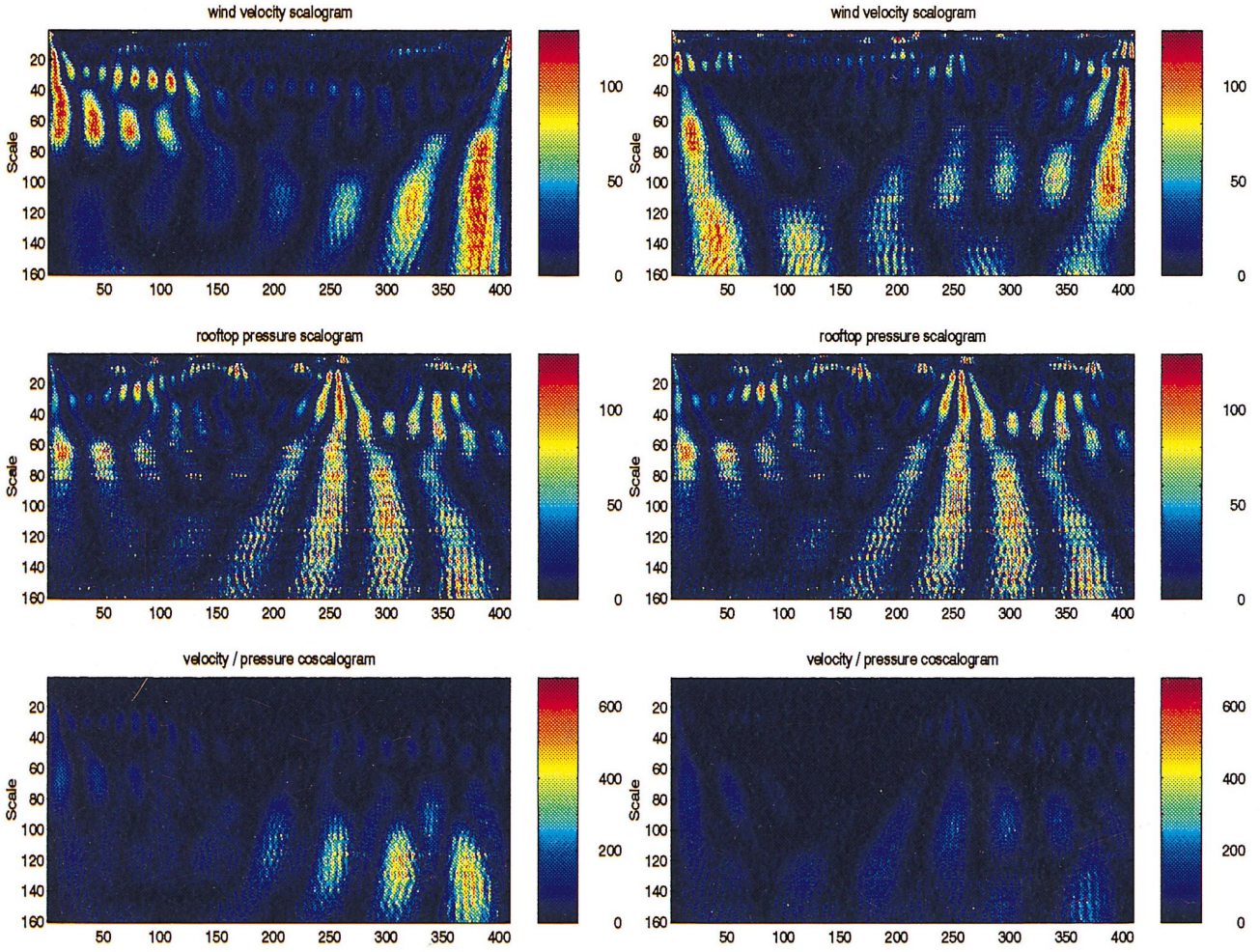

Fig. 12. Left: scalogram of upstream wind velocity and correlated rooftop pressure, and coscalogram of these two processes. Right: scalogram of uncorrelated wind velocity and pressure records, and the coscalogram of these two records.

approach flow with pressure fluctuations at a corresponding time instant. More carefully collected data in a controlled experiment is needed to further investigate this behavior.

2.4.5. Analysis of bridge response due to vortex shedding

A very instructive potential application of wavelet decomposition using the measured data in Reference 19 can be seen concerning the response behavior of a bridge due to vortex shedding. In their paper the authors note that spectral methods of data analysis are not very helpful due to non-stationarity of the measured data. To understand the behavior of the system the transition between regular and large amplitude response needs to be investigated. The spectral methods with constant bandwidth schemes do not permit zooming in time without losing resolution in frequency. The authors attempt to overcome the shortcomings of the spectral approach by decomposing energy into different structural modes, using a finite element model of the bridge to estimate the mode shapes of the three dominant modes of vibration. Fitting these mode shapes to the bridge response, they are able to approximate shifts in the relative contributions of the three modes as the response entered larger amplitude transient phases. Their investigation of response analysis can be aided through wavelet analysis as their data suggests changes in turbulence structure and switching of response from one mode of oscillation to another during their measurements.

Wavelet analysis is applied to a measured acceleration record made available by the authors of Reference 19. A modal analysis of the bridge separates the response into three main contributing modes which are first vertical, first torsional, and second vertical (~0.51, 0.74 and 0.81 Hz, respectively) [19]. A spectral analysis of the record shows the majority of response energy is due to the first vertical mode, but cannot reveal any changes in relative mode contributions in time. Fig. 13 shows a measured acceleration record with transient bursts of large amplitude response in the top plot, a scalogram of that record over a large range of scales (frequencies) in

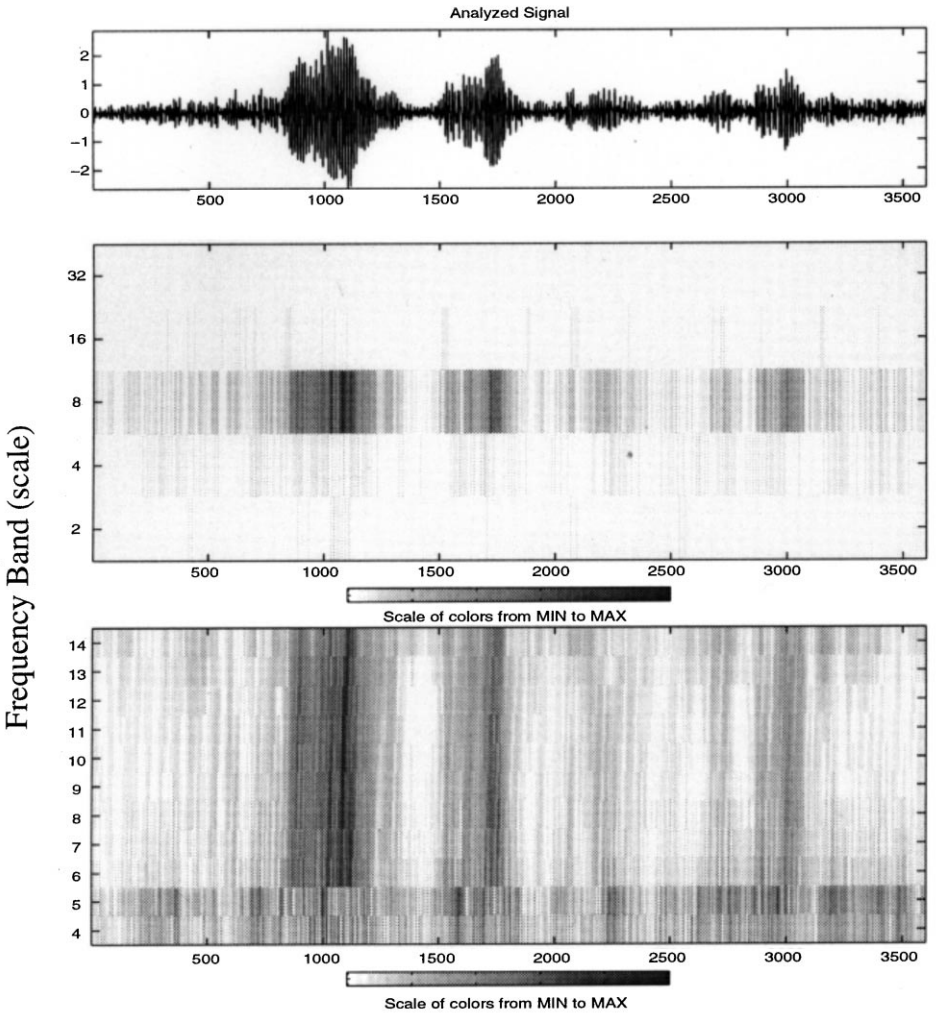

Fig. 13. Mesured bridge acceleration under the effect of vortex shedding, scalogram of response on course scale grid, and scalogram of same record on fine scale grid.

the middle plot, and a second more detailed scalogram over a smaller scale range in the bottom plot. Level 8 on the horizontal scale axis of the middle plot represents the frequency range of the first vertical mode of vibration (~0.51 Hz), and level 4 covers the frequency range of the two higher frequency modes. The darkest bands, representing large energy increases, can be seen in level 8, corresponding to the large amplitude bursts in the response record. The energy in the 4th level is more evenly distributed, showing no drastic increase associated with the large amplitude response.

The scalogram in the bottom plot is over a more narrow range of scales, and includes only the frequency range of the three modes of vibration. Here oversampling is employed using continuous wavelets to capture more detail. Levels 4 and 5 are now associated with the two higher modes of vibration, and levels 6 through 14 encompass the first mode of vertical vibration. Here it is more clearly seen that the energy content of the lowest frequency mode is strongly correlated with the large amplitude response, while the energy of the second and third modes is more evenly distributed through both low and high amplitude response. It is also noteworthy that a change in turbulence intensity of the approach flow may change the vortex excited loads, thus changing associated response. This observation was made based on full-scale data not reported here.

We can conclude that there is a strong shift to the first mode vibration for large amplitude response, and the higher modes of vibration make larger relative contributions to response at lower amplitudes. This was also concluded by the authors of Reference 19. Note however that the application of wavelet analysis eliminated the need for a finite element modal analysis. Spectral analysis is used to identify the major modes, and wavelet analysis is used to delineate their contributions in time.

2.5. Wavelet simulation of non-stationary processes

The retention of both time and frequency information makes wavelets a useful tool for the simulation of non-

stationary signals. This can be done given either a parent non-stationary signal, or a target spectrum and modulator function for each octave. Given a parent non-stationary signal, e.g. a local wind velocity record, an ensemble of signals may be simulated whose average statistics closely resemble those of the parent process. The parent signal is discrete wavelet transformed (DWT), and the coefficients are multiplied by a Gaussian white noise of unit variance $w(n)$. The inverse wavelet transform (IWT) then produces a simulation statistically similar to the parent process.

$$\hat{x}(n) = \mathrm{IWT}(w(n)^*\mathrm{DWT}(x(n))) \tag{7}$$

The concept of a modulated stationary process centered at narrow-banded frequencies to model ground motion has been used extensively [7,20–25]. In this representation each component process is modulated by a different modulating function,

$$x(t) = \sum_j m_j(t)s_j(t) \tag{8}$$

where m_j and s_j represent the jth modulator and the stationary component process, respectively. There are different approaches to modelling m_j and s_j to describe x. One such choice is to normalize the modulator such that

$$\int_{-\infty}^{\infty} m_j^2(t)\,\mathrm{d}t = 1 \tag{9}$$

and s_j is constant over a frequency band.

The DWT provides an elegant framework to perform such modelling [23,26]. The measured wavelet coefficients $a_{i,j}$ and spectrum may be used to estimate the modulator function from a parent signal by applying

$$m_{i,j} = A_i \sqrt{2^{i+2-M}}\,\frac{|a_{i,j}|}{\sqrt{S_i}} \tag{10}$$

where A_i is a level-dependent amplitude constant and S_i is the energy corresponding to the ith octave from the power spectrum. An example of identified modulator functions using equation (10) is given in Fig. 14. Here an earthquake ground motion record is broken into octave bands using DWT, the filtered time histories of several bands are shown along with the resulting modulator function.

Given a target spectrum and modulator functions, the simulation is done by first finding the energy contained in each octave from the target spectrum. The wavelet coefficients for the simulated process are multiplied with the appropriate modulator, and normalized such that the energy equals that in the corresponding octave. These modulated and normalized coefficients are then multiplied through by white noise and inverse wavelet transformed. The process is represented by [26]

$$\hat{x}(n) = \mathrm{IWT}\left(w(n)^*\left(\frac{m_{i,j}\sqrt{S_i}}{\sqrt{2^{i+2-M}}}\right)\right) \tag{11}$$

Fig. 15 shows a measured and a wavelet simulated earthquake ground motion record, and Fig. 16 compares the power spectral density of both records. Both the non-stationary characteristics and the energy distribution are well represented in the simulation. Fig. 17 is an example of measured non-stationary wind velocity and a wavelet simulation. Again the non-stationary characteristics are well represented.

2.6. Denoising

Small details in a signal are manifested in the wavelet transform as small magnitude coefficients. These low energy processes may distort the true signal if they are assumed to be due to noise. Their removal is accomplished in the wavelet domain by eliminating or reducing coefficients under a certain magnitude threshold. The inverse wavelet transform then gives back a 'cleaned' or denoised signal without the small details in the original signal. Two thresholding methods considered here are hard and soft thresholding.

Hard thresholding sets to zero the coefficients below the threshold through

$$a_{i,j}^{\mathrm{hard}} = \begin{pmatrix} 0, a_{i,j} < \lambda \\ a_{i,j}, a_{i,j} \geq \lambda \end{pmatrix} \tag{12}$$

where λ is the assigned threshold. Soft thresholding alters the coefficients, for example

$$a_{i,j}^{\mathrm{soft}} = \mathrm{sign}(a_{i,j})\,(|a_{i,j}| - \lambda) + \tag{13}$$

where + indicates that if the sign of $a_{i,j}^{\mathrm{soft}}$ does not equal the sign of $a_{i,j}$, $a_{i,j}^{\mathrm{soft}}$ is set to zero [27]. Equation (13) results in a smooth reduction of all coefficients toward zero, and sets equal to zero those closest to the origin. Each method has advantages, depending on the properties of the signal being cleaned. An example of a threshold parameter defined in terms of noise level is found in Reference 27, and written as

$$\lambda = \sigma\sqrt{2\log(n)}/\sqrt{n} \tag{14}$$

where σ is a noise scale parameter, and n is the number of points in the signal.

For qualitative analysis, an iterative increase in the threshold will clean the signal to a desired level, but, as is the problem with all noise reduction methods, a trade-off between removing noise and removing important low

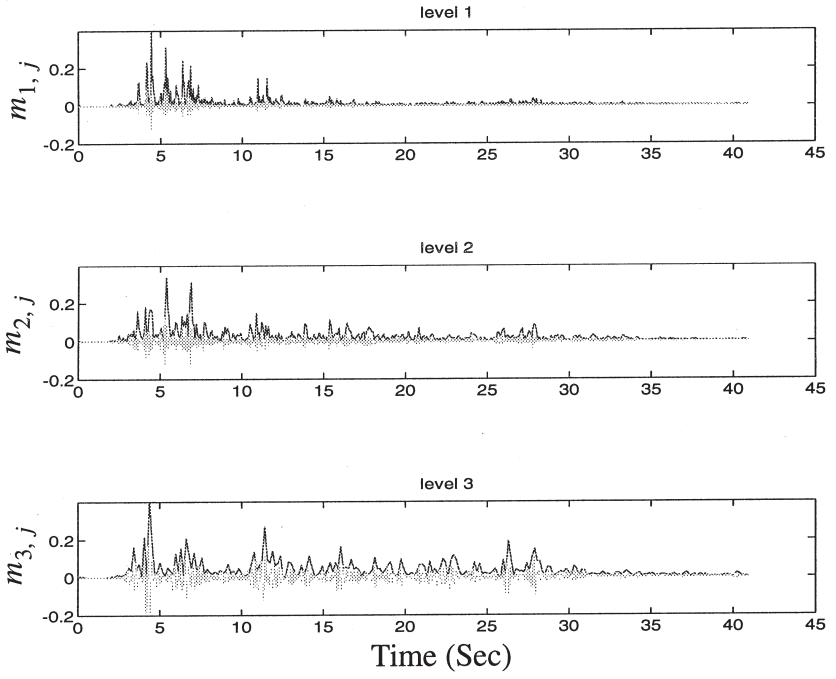

Fig. 14. Octave band filtered ground motion signals and their identified envelopes using DWT.

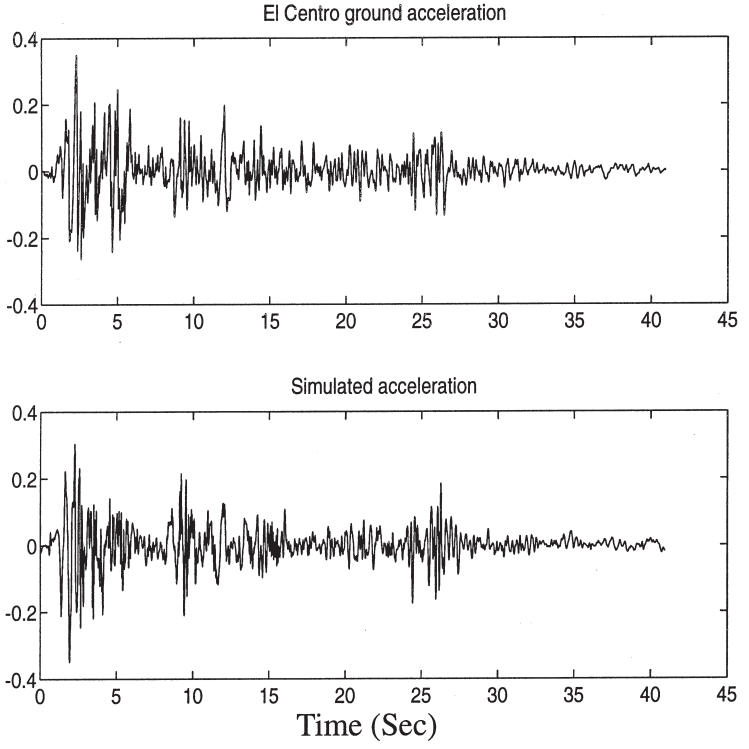

Fig. 15. Measured and simulated non-stationary ground motion signal using DWT.

energy information cannot be avoided. Some concept of the desired level of noise to be removed is thus necessary. For the purpose of demonstration, two signals are contaminated with noise such that both the noise and the desired clean signal are known exactly. A minimization of the mean squared error (MSE) is performed using soft and hard thresholding in which the optimal threshold parameter, λ_{opt}, for that signal is found, where

$$\text{MSE} = \frac{1}{N}\sum_{n=1}^{N^M}(f(n) - \hat{f}(n))^2 \tag{15}$$

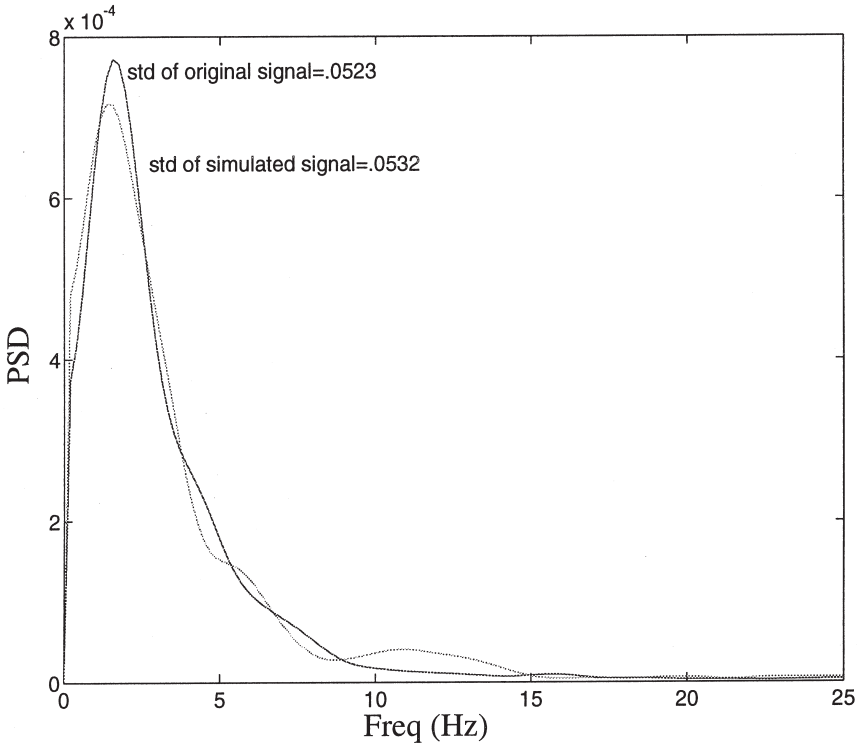

Fig. 16. Power spectral density of measured earthquake ground motion and wavelet simulated signals.

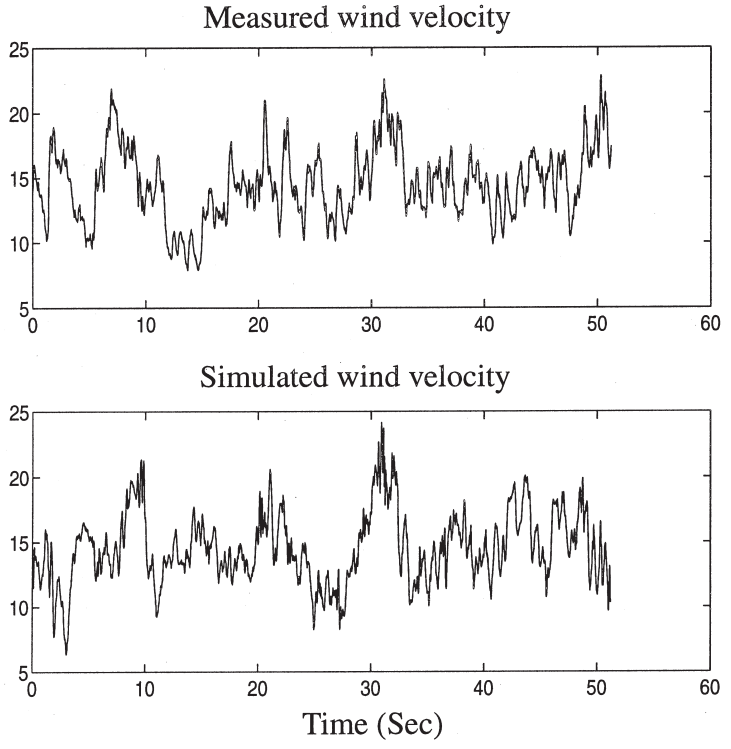

Fig. 17. Measured wind velocity and a simulation using DWT.

and

$$\min(\mathrm{MSE}) = \mathrm{MSE}(f,\hat{f}_{\mathrm{opt}}(\lambda_{\mathrm{opt}})) \tag{16}$$

Here, $f(n)$ is the uncontaminated signal, $\hat{f}(n)$ is the estimated clean signal from an inverse wavelet transform of the coefficients after thresholding at λ, and $\hat{f}_{\mathrm{opt}}(\lambda_{\mathrm{opt}})$ is the optimal estimated clean signal as a function of the optimal threshold value which minimizes the MSE.

Demonstrations of wavelet transform-based optimized noise removal are given in Figs. 18 and 19. In the top plot of Fig. 18 the uncontaminated signal is the superposition of two sine waves, the same signal is then contaminated with white noise. The contaminated signal is cleaned using soft and hard thresholding in the center and bottom plots, respectively. Both techniques apply minimization of the MSE between the uncontaminated signal and the iteratively estimated cleaned signal. Fig. 19 demonstrates the application of the wavelet denoising method using a measured wind pressure signal contaminated with added white noise. Both figures list the resulting minimum MSE along with the MSE between the original contaminated and uncontaminated signal. Hard thresholding better reduces the MSE for the first example, while the opposite is true for the second example. Denoising using wavelet techniques is typically performed using a pre-estimate of the noise level to establish the threshold.

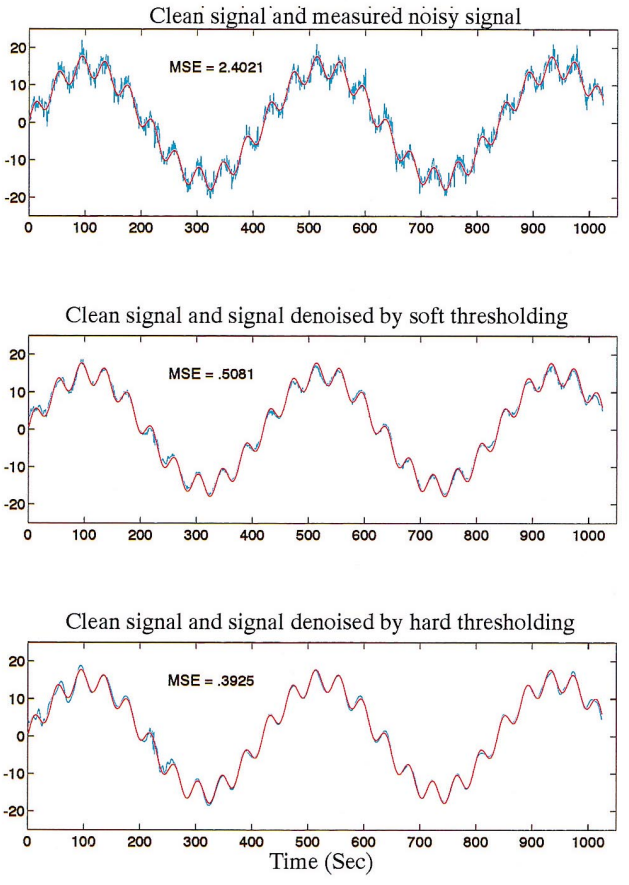

Fig. 18. Denoising of two superimposed sine waves contaminated by white noise using DWT thresholding.

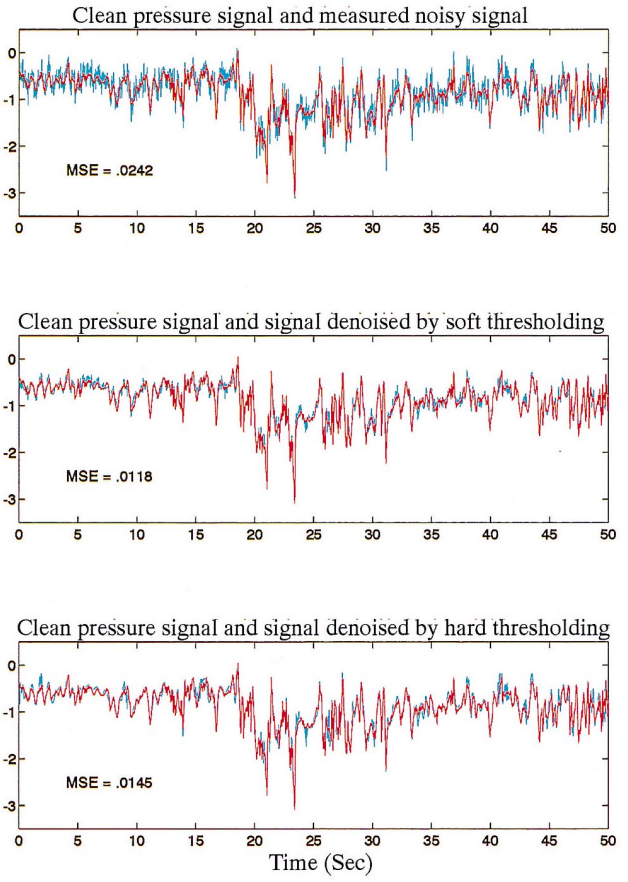

Fig. 19. Noise reduction of a pressure record contaminated by white noise using DWT thresholding.

3. Concluding remarks

Progress in quantifying and simulating non-stationary signals has been elusive due to the limitations of traditional analytical tools. The analysis and simulation of non-stationary processes involving wind, wave and earthquake applications is accomplished here by decomposition into localized basis functions via the discrete or continuous wavelet transform, whose popularity is growing as more researchers from a wide range of disciplines find their application useful. This paper briefly introduces the wavelet transformation and provides examples of their usefulness in spectral and cospectral analysis, time-scale decomposition for the identification of transient events, structural performance monitoring via the scalogram, non-stationary signal simulation, and the cleaning of noisy signals. Readers are encouraged to consult the reference list for a more

detailed mathematical treatment of wavelet decomposition.

Acknowledgements

The support for this work was provided in part by NSF Grants BCS-9096274 (BCS-8352223), CMS9402196, and ONR Grant N00014-93-1-0761. The first author ws partially supported by a Department of Education GAANN Fellowship during this study. Experimental data was provided by Texas Tech University, a joint offshore industry project, Tokyo Institute of Polytechnics, and the authors of Reference 19, their assistance is appreciated.

References

[1] Kareem A, Gurley K, Kantor JC. Time-scale analysis of nonstationary processes utilizing wavelet transforms. Proc 6th Int Conf Structural Safety and Reliability. Innsbruck, Austria, Balkema Publishers, Amsterdam, Netherlands, 1993.
[2] Farge M. Wavelet transforms and their applications to turbulence. Annual Rev Fluid Mech 1992;24.
[3] Daubechies I. Orthonormal basis of compactly supported wavelets. Comm Pure Appl Math 1988;41:909–96.
[4] Strang G. Wavelets and dilation equations: a brief introduction. SIAM Rev 1989;31(4):614–627.
[5] Newland DE. An introduction to random vibrations, spectral and wavelet analysis. Longman, New York, 1993.
[6] Mallat S. A theory for multiresolution signal decomposition: the wavelet representation. IEEE Trans Pattern Anal Machine Intell 1989;11:674–693.
[7] Kameda H. Evolutionary spectra of seismogram by multifilter. J Engng Mech Div, ASCE 1975;101(EM6):787–801.
[8] Rioul O, Duhamel P. Fast algorithms for discrete and continuous wavelet transforms. IEEE Trans Inf Theory 1992;38:569–586.
[9] Coifman RR, Wickerhauser MV. Entropy-based algorithms for best bias selection. IEEE Trans Inf Theory 1992;38(2):713–718.
[10] Misiti M, Misiti Y, Oppenheim G, Poggi JM. Wavelet toolbox users guide: for use with MATLAB, The Math Works, 1996.
[11] Sadowsky J. Investigation of signal characteristics using the continuous wavelet transforms. Johns Hopkins APL Technical Digest 1996;17(3):258–269.
[12] Scherer RJ. On the frequency dependence of the strong ground motion duration. Structural safety and reliability, Schueller, Shinozuka and Yao (editors), Balkema Publishers, Rotterdam, 1994:2201–2223.
[13] Hodges CH, Power J, Woodhouse J. The use of sonogram in structural acoustics and an application to vibrations of cylindrical shell. J Sound Vibr 1985;101(2):203–218.
[14] Broglie, Louis de Heisenberg's uncertainties and the probabilistic interpretation of wave mechanics. Kluwer, Boston, 1990.
[15] Kareem A, Hsieh CC, Tognarelli MA. Response analysis of offshore systems to nonlinear random waves part I: wave field characteristics. Proc Special Symp Stochastic Dynamics and Reliability of Nonlinear Ocean Systems. Ibrahim and Lin (editors), ASME, Chicago, IL, 1994.
[16] Wahl TJ, Bolton JS. The application of the Wigner distribution to the identification of structure-borne noise components. J Sound Vibr 1993;163(1):101–122.
[17] Arnold CR. Spectral estimation for transient wave forms. Int Electrical and Electron Engineers Trans Audio Electroacoust 1970;AU-18(3):248–257.
[18] Scherer RJ, Riera JD, Schueller GI. Estimation of the time-dependent frequency content of earthquake accelerations. Nucl Engng Des 1982;71:301–310.
[19] Owen JS, Vann AM, Davies JP, Blakeborough A. The prototype testing of Kessock bridge: response to vortex shedding. J Wind Engng Indust Aerodynam 1996;60:91–106.
[20] Saragoni GR, Hart GC. Simulation of artificial earthquakes. Earthq Engng Struct Dynam 1974;2:249–267.
[21] Grigoriu M, Ruiz SE, Rosenblueth E. Nonstationary models of seismic ground acceleration. Nat center for earthquake engineering research, Technical report NCEER-88-0043, 1988.
[22] Der Kiureghian A, Crempien J. An evolutionary model for earthquake ground motion. Struct Safety 1989;6:235–246.
[23] Pinto AV, Pegon P. Numerical representation of seismic input motion. Experimental and numerical methods in earthquake engineering, Donea and Jones (editors), ECSC, EEC, EAEC, Brussels and Luxembourg, 1991.
[24] Li Y, Kareem A. Simulation of multivariate random processes: hybrid DFT and digital filtering approach. J Engng Mech, ASCE 1993;119:1078–1098.
[25] Li Y, Kareem A. Simulation of multivariate nonstationary random processes by FFT. J Engng Mech, ASCE 1991;117:1037–1058.
[26] Gurley K, Kareem A. On the analysis and simulation of random processes utilizing higher-order spectra and wavelet transforms. Proc 2nd Int Conf Computational Stochastic Mechanics, Athens, Greece, Balkema Publishers, Amsterdam, Netherlands, 1994.
[27] Vidakovic B, Muller P. Wavelets for kids, a tutorial introduction. Wavelet Digest 1991.